ACCOUNTS of chemical research

Article

pubs.acs.org/accounts

# Achievements of DFT for the Investigation of Graphene-Related Nanostructures

Andrés R. Botello-Méndez,* Simon M.-M. Dubois, Aurélien Lherbier, and Jean-Christophe Charlier

Institute of Condensed Matter and Nanosciences, Université catholique de Louvain, Chemin des étoiles 8, 1348 Louvain-la-neuve, Belgium

**CONSPECTUS:** Graphene-related nanostructures stand out as exceptional materials due to both their wide range of properties and their expanse of interest in both applied and fundamental research. They are good examples of nanoscale materials for which the properties do not necessarily replicate those of the bulk. For the description and the understanding of their properties, it is clear that a general quantum-mechanical approach is mandatory. The remarkable result of density functional theory (DFT) is that the quantum-mechanical description of materials at the ground state is made amenable to simulations at a relatively low computational cost.

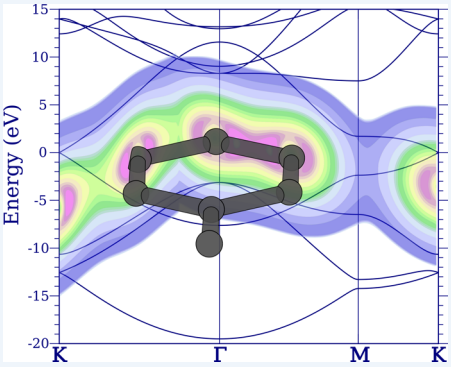


The knowledge of materials has undergone a revolution after the introduction of DFT as an unrivaled instrument for the investigation of materials properties through computer experiments. Their deeper understanding comes from a variety of tools developed from concepts intrinsically present in DFT, notably the total energy and the charge density. Such tools allow the prediction of a diverse set of physicochemical properties relevant for material scientists.

This *Account* lays out an example-driven tour through the achievements of *ground-state* DFT applied to the description of graphene-related nanostructures and to the deep understanding of their outstanding properties. After a brief introduction to DFT, the survey starts with the determination of the most basic properties that can be obtained from DFT, that is, band structures, lattice parameters, and spin ground state. Next follows an exploration of how total energies of different systems can give information about relative stability, formation energies, and reaction paths. Exploiting the derivatives of the energy with respect to displacements leads the way toward the extraction of vibrational and mechanical properties. In addition, a close examination of the charge density gives information about charge transfer mechanisms, which can be linked to chemical reactivity. The ground state density and Hamiltonian finally connect to the concepts behind transport phenomena, which drive much of the application-oriented research on graphene and graphene-related nanostructures. In each section, a selection of cases that are of current importance are used to illustrate the use and relevance of DFT-based techniques. In summary, this *Account* presents an introductory landscape of the possibilities of *ground-state* DFT for the study of graphene-related nanostructures. The prospect is rich, and the use of DFT for the study of graphene-related nanostructures will continue to be fruitful for the advancement of these and other materials.

## 1. THE DENSITY FUNCTIONAL THEORY (DFT) FRAMEWORK

The nonrelativistic quantum state of matter is established once the wave functions that solve the many-body Schrödinger equation are found. However, the problem as stated directly from the Schrödinger equation is too complex to be numerically solved when the system contains more than a few atoms. A first simplification comes from the Born−Oppenheimer approximation.[1] The electron and nuclei dynamics are decoupled by taking advantage of the large masses of nuclei. In order to deal with the electronic system, Hohenberg and Kohn (HK) introduced a formulation where the electron density distribution, instead of the many-body wave function, plays the central role.[2,3] They envisioned a variational expression for the energy as a functional of the density that is to be minimized to find the quantum ground-state of the system. Eventually, Kohn and Sham (KS) proposed a practical scheme to evaluate the density functional. In this formulation, the many-body nature of the problem is encapsulated in an exchange-correlation (XC) potential, which is at the heart of both the successes and failures of DFT.[4] Useful review papers are found in refs 3, 5, and 6. The ground-state many-body wave function is built upon non-interacting electronic eigenstates, called Kohn−Sham orbitals, evolving in a self-consistent field derived from the XC potential. It is noteworthy that if the XC functional that is used were exact, then DFT would perfectly describe the quantum nature of matter. Over the years, DFT has been extended to the study of response functions and many-body problems by means of frameworks such as density functional perturbation theory (DFPT), time-dependent density functional theory, or the GW

**Special Issue:** DFT Elucidation of Materials Properties

**Received:** August 1, 2014
**Published:** October 28, 2014

   dx.doi.org/10.1021/ar500281v | *Acc. Chem. Res.* 2014, 47, 3292−3300

approximation.[7−10] Nonetheless, simple approximations for the XC functional yield remarkably good results that allow one to describe many relevant properties of materials.

Various basis sets are used to expand the KS wave functions. Plane-waves (PWs) are a common choice. Indeed, PWs naturally account for the periodicity of crystals[11] and naturally suit the description of nearly free electrons. In addition, they form an orthogonal basis set whose completeness can be systematically increased by adding PWs of higher kinetic energy. In contrast, PWs can become computationally expensive for the description of low dimensional or highly inhomogeneous systems. An alternative comes from linear combination of atomic orbitals (LCAO). LCAO appears as a natural method to describe the binding of atoms in crystals or molecules. Its main caveat is the lack of a systematic procedure to improve the accuracy of the representation, which may induce a lack of transferability.

## 2. ELECTRONIC STATES AND BAND STRUCTURES

In crystal structures, electrons move in a periodically repeating potential, and thus the KS orbitals are Bloch waves. The electronic structures of these systems are characterized by the band structure, which summarizes the energy dependence on momenta, $k$, that is, solving the KS equations at different $k$ along a convenient high symmetry path. The eigenvalues of the problem are interpreted as the energy bands and the eigenfunctions as the KS wave functions. The density of states is the integration of all possible momenta and represents the available states per unit of volume at a given energy. The band structure of graphene is illustrated in Figure 1a, which is calculated using either PWs (solid black) or LCAOs (dashed red lines). The validity of the use of local density (LDA) and generalized gradient (GGA) functionals for carbon is evidenced when compared with the many body band structure (GW approximation). There is a set of bands associated with nearly free electron states that are not present in the LCAO band structure. LCAO fails to account for those bands since nearly free electrons extend in the vacuum and are difficult to understand in terms of C atomic orbitals.[12]

## 3. LATTICE PARAMETERS AND GEOMETRY OPTIMIZATION

Within the Born−Oppenheimer framework, whether a simple relaxation or a full ionic trajectory is under consideration, the nuclei coordinates are propagated according to the forces computed in the ground-state electronic configuration. The ionic forces are straightforwardly computed by means of the Hellmann−Feynman theorem.[14,15]

The equilibrium lattice parameters of a crystalline system are those that minimize its total energy. The accuracy of these calculations depends on the XC used.[16] While local and semilocal XC functionals usually provide an accurate description of covalent and ionic chemical bonds, they usually fail to reproduce nonlocal dispersive interactions, for example, van der Waals (vdW), which are important in weakly bonded materials such as $sp^2$ carbon materials. These discrepancies are illustrated in Figure 1b, where all curves have been referenced to the ground state energy ($E_{GS}$) for comparison. The relevant comparison is with respect to the depth of potential well and the exfoliation energy, $E_{xfol}$, defined as the difference of total energy between the bound graphite system and the isolated layers (i.e., $E_{Tot}$ when the interlayer distance tends to infinity).

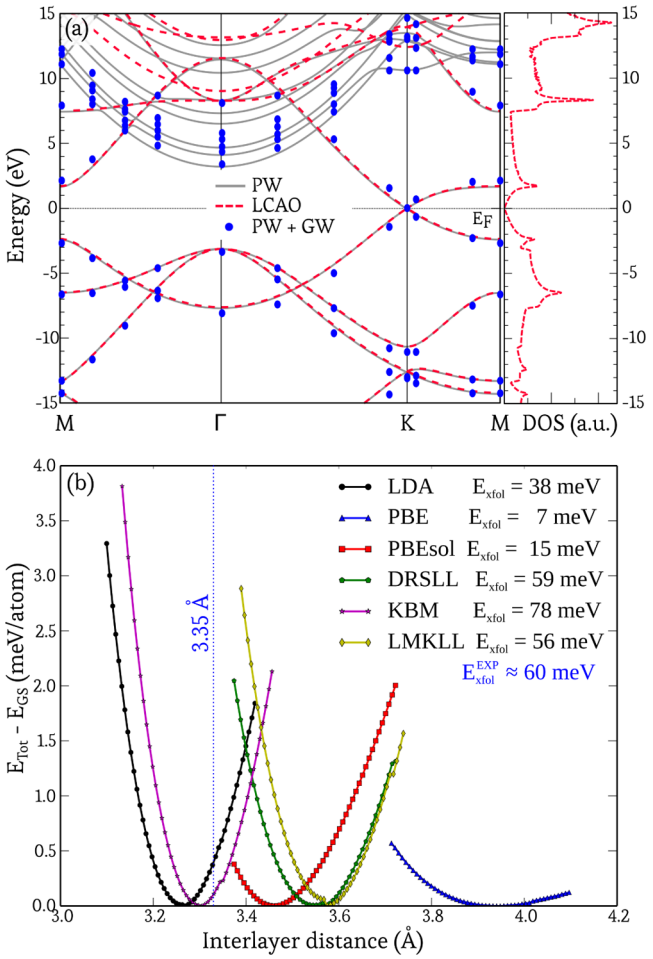


**Figure 1.** (a) Electronic band structure of graphene calculated using a plane-wave basis set (black lines) and a localized basis set (dashed red lines). The many-body GW results represented by blue dots are adapted from ref 13. (b) Comparison between different functionals for the calculation of the interlayer distance ($d$) and the exfoliation energy ($E_{xfol} = E_{Tot}(d \to \infty) - E_{GS}$) of graphite.

We have compared LDA,[17] with different flavors of GGA (PBE[18] and PBEsol[19]) and vdW functionals (DSRLL,[20] KBM,[21] and LLMKL[22]). The experimental value for the layer−layer distance in graphite is ca. 3.37 Å,[23] and the exfoliation energy has been reported from thermal desorption measurements to be 60 meV/atom.[24] Note that GGAs predict very small or no binding at all. LDA functionals describe surprisingly well the binding of graphite, even though there are no terms to account for vdW interactions. However, LDA cannot be considered as a reliable approximation for other systems, such as graphene on metals, which are of considerable importance.[25,26]

## 4. SPIN POLARIZATION AND SPIN−ORBIT COUPLING

The original Hohenberg−Kohn−Sham theory did not include explicitly the spin of the electrons.[2,4] However, the generalization was quickly achieved.[27,28] In this case, it suffices to construct spin-dependent effective potentials, as well as equations for the spin-resolved (or spinor for the case of non-collinear spin) KS orbitals.[27]

The ground-state of ideal $sp^2$ carbon nanostructures is nonmagnetic. However, the idea of having magnetic states in such a light element has attracted the interest of theoreticians


dx.doi.org/10.1021/ar500281v | Acc. Chem. Res. 2014, 47, 3292−3300

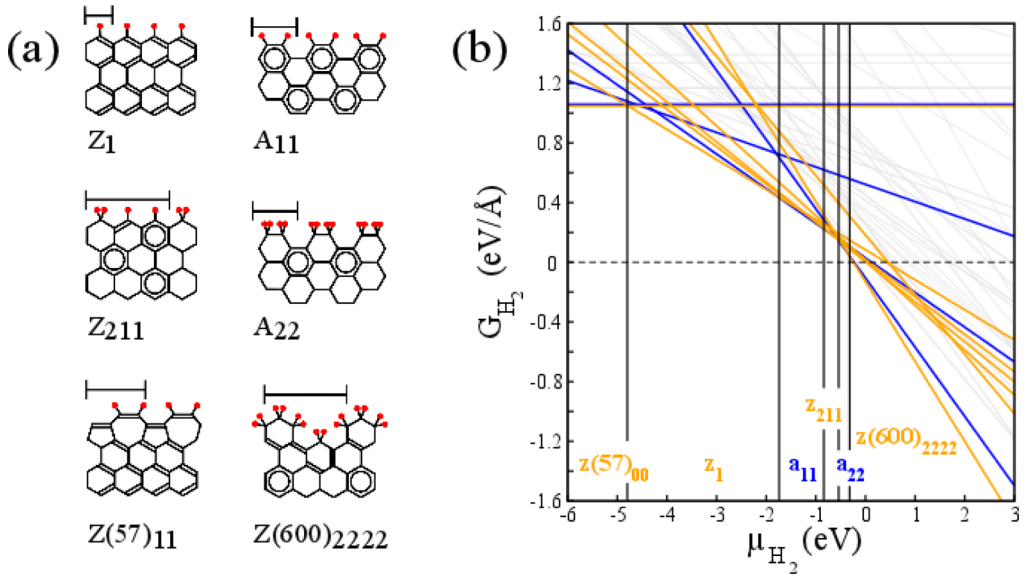


**Figure 2.** (a) Schematic representation of the most stable edge reconstructions of armchair and zigzag nanoribbons. The length of the unit cell is represented by a line segment. Carbon and hydrogen atoms are depicted, respectively, in black and red. (b) Phase diagrams, i.e. edge free energies as a function of the $H_2$ chemical potential. Blue and orange lines, respectively, depict the most stable armchair and zigzag reconstructions. Vertical lines are used to delineate the stability windows. Gray lines represent all the considered configurations found as metastable.

and experimentalists, with its own amount of controversy. The observed magnetic properties in graphitic materials are often attributed to the presence of impurities, defects, or boundaries.[29] Besides the relatively obvious magnetic impurities,[30] other lighter elements have been shown to induce spin polarization in graphene.[31] Computations of isolated vacancies have also shown spin-polarized states.[31] At the edges of a strip or nanoribbon (NR) of graphene, magnetic states have been predicted to appear if the edge shape is zigzag. The particular magnetic orientation is ferromagnetic along the edges and antiferromagnetic between the edges.[32] Similar edge states can occur at grain boundaries.[33,34]

Relativistic effects in carbon nanostructures are, for most purposes, negligible since carbon is a light atom. Low-energy carriers in graphene have weak spin−orbit coupling (SOC). The energy gap arising from the intrinsic SOC is estimated to be about 25 $\mu$eV only, and large spin relaxation times of several microseconds are predicted.[35,36] Hence, graphene materials are considered promising candidates for spintronic devices.[37] However, there are some cases in which it is important to consider the spin−orbit interaction. This is done by adding to the KS equations a spin−orbit term of the generic form $|l,s\rangle \mathbf{L}\cdot\mathbf{S}\langle l,s|$, where $\mathbf{L}$ and $\mathbf{S}$ are the angular and spin momentum operators. SOC should be considered in graphene when the layer is curved or under external fields (Rashba interaction).[38,39] Small amounts of adatoms have also been shown to increase the spin−orbit interaction of graphene by several orders of magnitude.[40]

## 5. FORMATION ENERGIES

The comparison of total energies can give us information about the relative stability of different configurations. A problem of interest is the edge termination of graphene nanoribbons (NRs), because their electronic properties heavily depend on the exact shape and passivation of the edges. Nanoribbons are classified into zigzag (Z) and armchair (A) ribbons depending on the shape of their edges. Depending on the edge passivation, ZNRs may exhibit edge states not present in ANRs. These edge states exhibit ferromagnetic ordering along the edge,[32] which has attracted much attention for spin-related applications. The edge formation energy of hydrogen passivated nanoribbons, given per edge length ($a$),

$$\xi_{H_2} = \frac{1}{2a}\left(E_{NR} - N_C\frac{E_{graphene}}{2} - N_H\frac{E_{H_2}}{2}\right) \quad (1)$$

describes the relative stability of the isolated systems at zero temperature. However, the edge formation energies $\xi_{H_2}$ do not account for the environmental conditions present in most experiments, notably the pressure and temperature during synthesis and processing. The relative stability in realistic conditions is ruled by the edge free energy.[41] In the case of hydrogen passivated nanoribbons, the chemical potential $\mu_{H_2}$ is the main variable of interest. In the athermal limit, that is, assuming that the temperature dependency of graphene and nanoribbon free energies is negligible, the edge free energy can be approximated as[41,42]

$$G_{H_2}(T, P) \simeq \xi_{H_2} - \left(\frac{N_H}{2a}\right)\frac{\mu_{H_2}}{2} \quad (2)$$

Figure 2b sketches the dependency of the edge free energy with respect to $\mu_{H_2}$ for a large set of reconstructions of the zigzag and armchair edges. For comparison, one notes that in ambient conditions ($P$ = 1 bar and $T$ = 300 K), the partial pressure is about $5 \times 10^{-7}$ bar, leading to a value of $\mu_{H_2} \simeq -0.69$ eV. The computed phase diagrams strongly contrast with the widely spread idea that armchair shaped edges are globally more stable. The most stable structures are depicted in Figure 2a. At 300 K, for standard and high hydrogen partial pressure ($P_{H_2} > 5 \times 10^{-10}$ bar), three edge configurations are particularly relevant, namely, the $Z_{211}$, $A_{22}$, and $Z(600)_{2222}$ patterns. The most commonly studied $A_{11}$ and $Z_1$ edge structures appear to be stable only at low and very low hydrogen concentrations ($P_{H_2} < 5 \times 10^{-10}$ bar).


dx.doi.org/10.1021/ar500281v | Acc. Chem. Res. 2014, 47, 3292−3300

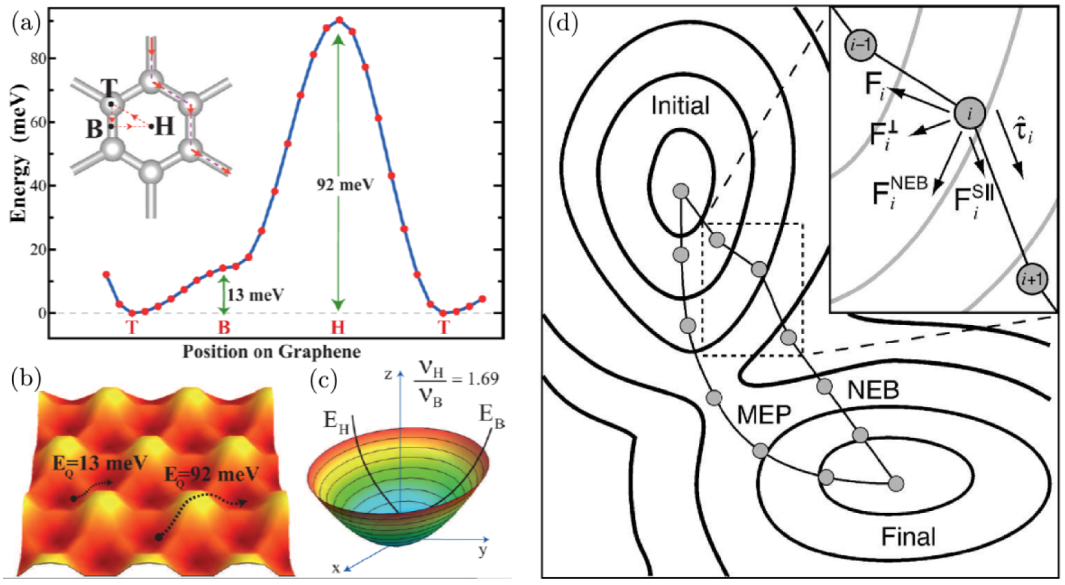


**Figure 3.** (a) Energy barriers for a single Cl adatom moving along the high symmetry path of a hexagon (top (T), bridge (B), and hollow (H) positions). The diffusion path with the lowest energy barrier (13 meV) is indicated by thick red dashed lines in the inset. (b) Corresponding energy landscape. Dark (light) color represents the top (hollow) sites. (c) Potential energy contour plots (paraboloid) of Cl adatom around the T-site. The jump frequencies of Cl atom $\nu$ for different directions are calculated from this paraboloid. (d) Illustration of the NEB method for finding MEP going through an energy saddle point. Panels a, b, and c are courtesy of H. Şahin, reprinted with permission from ref 43. Copyright 2012 American Chemical Society. Panel d is courtesy of D. Sheppard, reprinted with permission from ref 47. Copyright 2008 AIP Publishing.

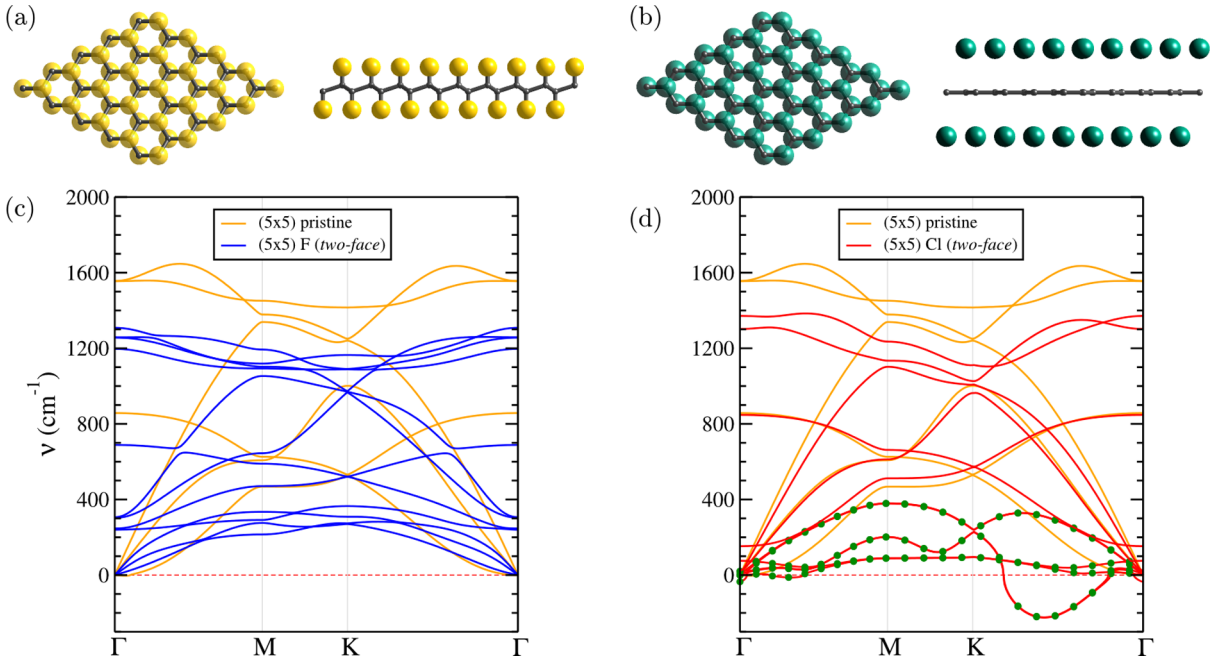


**Figure 4.** Geometries and phonon band structures of *two-face* fluorinated (a, c) and chlorinated (b, d) graphene. In panels c and d, the phonon band structures of pristine graphene (given as references) are depicted in orange. In panel d, the bands associated with the vibration modes of the two weakly bonded layers of chlorine atoms are highlighted by green circles.

## 6. MINIMAL ENERGY PATH

The minimal energy path (MEP) between an initial and a final is an information that can be directly inferred from the total energies obtained from DFT calculations. Often, not only the stable conformations and preferential anchoring positions of a surface adatom, a cluster, or a molecule are a valuable knowledge, but also their diffusion path through the material and associated reaction rate. The direct approach consists of computing from total energy calculations the complete potential energy surface of a system, from which potential barriers and hence the MEP can be deduced. This situation is illustrated in Figure 3a−c for the simple case of a single chlorine adatom deposited on a graphene layer.[43] The stable position is on top (T) of a carbon atom. In the hollow (H) position, the Cl adatom is unstable, and the bridge (B) position is a saddle point (Figure 3b). The energy barrier between the stable T and the B (H) position is 13 meV (92 meV). The barrier analysis allows one to determine along which path


dx.doi.org/10.1021/ar500281v | Acc. Chem. Res. 2014, 47, 3292−3300

chlorine adatoms mostly diffuse (inset of Figure 3a) and at what rate (Figure 3c), which is quite high since diffusion barriers are found to be very small.[43] In most cases, the complexity and number of degrees of freedom prevent the calculation of the full potential energy surface. Therefore, a more sophisticated approach such as the nudged elastic band (NEB) method is required.[44,45]The NEB method iteratively searches the MEP from a discretized number of images obtained from a linear interpolation of the initial and final geometries (from NEB line to MEP in Figure 3d). At each iteration, the images are relaxed. To guarantee that all the images relax to the same MEP, fictitious springs are added. The MEP is found when the NEB forces ($F_i^{NEB}$), that is, the sum of the perpendicular component of the true forces ($F_i^{\perp}$) and the parallel compononent of the spring forces ($F_i^{S\parallel}$), have been minimized. The NEB method has, for instance, been used to investigate graphene growth and healing of defects.[46]

## 7. PHONON DISPERSION

Besides the geometry optimization, the vibrational eigenmodes of a crystal can be determined from the first derivative of forces with respect to ionic displacement, that is, second derivative of energy (Hessian matrix). The phonon band structure can be calculated using either the small displacement method (SDM) or a linear response function (LRF) approach.[8] Within the SDM, also called the frozen phonon technique, atoms are slightly displaced from their stable positions in each principal direction. The induced forces on neighboring atoms are then used to build the corresponding dynamical matrix whose eigenvalues and eigenstates are the phonon frequencies and vibration modes, respectively. In the other hand, the LRF approach computes directly the second derivatives of the energy based on linear response of the density as described within the DFPT.

Phonon band structure provides information about the lattice stability with respect to collective ionic displacements. This is illustrated in Figure 4, which compares phonon dispersion curves for the unit cell of pristine graphene and *two-face* functionalized graphene. The phonon band structures of fluorinated graphene, whose structure is depicted in Figure 4a, reveals only positive eigen-frequencies (blue curves in Figure 4c). Hence, the crystal is found to be locally stable. In contrast, imaginary phonon frequencies are calculated for the chlorinated graphene structure depicted in Figure 4b. These eigen-frequencies (plotted as negative values in Figure 4d) attest to the unstable character of the simulated geometry. In this case, the interactions between the densely packed chlorine atoms, which are only weakly bonded to graphene, are responsible for the phonon instability. The unstable phonons correspond to vibrations of the chlorine layers, while the modes associated with the carbon plane are very similar to the case of pristine graphene. H. Şahin and S. Ciraci have reported a locally stable buckled structure of *two-face* chlorinated graphene that is free of phonon instabilities.[43]

Vibrational modes are also very useful to guide the interpretation of vibrational spectroscopies, including neutron scattering experiments as well as infrared and Raman spectroscopies, which are particularly widely used for the characterization of carbon nanostructures.[48,49]

## 8. ELASTIC CONSTANT AND MODULI

After the calculation of forces and vibrational properties, it is inevitable to wonder about the mechanical properties of materials, especially for $sp^2$ carbon derivatives, whose bond has been suggested to render materials with the highest strength. The calculation of the Young modulus, and of the elastic constants involves the second derivative of the energy with respect to strain. It is important to note that the definition of the elastic moduli depends on the volume of the system, which in the case of graphene nanostructures is not always trivial. For instance, in the case of carbon nanotubes, there has been some discrepancies on the definition of the volume of either a solid or a hollow cylinder with different thicknesses.[50−52] In order to be able to compare with graphene, the convention is to take a hollow tube with a thickness equal to the interlayer spacing in graphite.

The DFT calculated elastic constants are usually in good agreement with experiment;[53,54] however it should be considered that the modes involving out of plane interactions (i.e., $C_{33}$ and $C_{44}$) should be calculated incorporating vdW corrections. Besides the good predictive ability that these tools have brought for the elastic moduli of nanotubes,[50,51] there has been recent interest in studying the shear constant of graphene, since it is involved in important aspects of its fabrication, such as exfoliation.[53,55] In this respect, recent comparisons reveal that LDA and GGA can reproduce the experimentally measured shear constant $C_{44}$ for few layer graphene, as long as the interlayer spacing used is obtained from calculations accounting for vdW interactions.[55]

## 9. CHARGE TRANSFER

The electronic density computed from DFT can give information about the nature of chemical bonds (electronegativity, covalency, ionicity) through the charge transfer between atoms, that is, the way the electronic cloud is rearranged when atoms bind with each other. However, it is not trivial to assign electrons to a given atom of a material (or a molecule) since charge density is a priori defined everywhere. One of the most well-known and oldest methods is the Mulliken population analysis.[56,57] This method is not based on the real-space representation of the electronic density but is derived instead from the LCAO approach. The wave functions are expanded on localized basis functions, $\psi_\alpha(\mathbf{r}) = \sum_\mu c_\mu^\alpha \phi_\mu(\mathbf{r})$, where $\alpha$ is the band index and $\mu$ is the orbital index. The atomic charge, which is the difference between the nuclear charge ($Z_i$) and the charge attributed to the atom $i$ in the material, is computed from the density matrix coefficients ($\rho_{\mu\nu} = \sum_\alpha n_\alpha c_\mu^\alpha c_\nu^\alpha$) and the overlap matrix elements ($S_{\mu\nu} = \langle \phi_\mu | \phi_\nu \rangle$) as

$$Q_i = Z_i - \sum_{\mu \in i,\nu} \rho_{\mu\nu} S_{\nu\mu} \tag{3}$$

The major drawback of this approach is the strong dependency on the choice of the basis set possibly yielding an unrealistic atomic charge.[58] The other types of methods are all based on real-space representation of the electronic density ($\rho(\mathbf{r})$), such as the Hirshfeld method,[58,59] the Bader analysis,[60,61] and the Voronoi deformation density (VDD).[58,62] These methods distinguish themselves by a different spatial partitioning of $\rho(\mathbf{r})$ around the atoms. In the case of Bader analysis, the space partition is determined from the topology of $\rho(\mathbf{r})$ using its minima and its gradient. The Hirshfeld and VDD methods are close to each other and utilize


dx.doi.org/10.1021/ar500281v | Acc. Chem. Res. 2014, 47, 3292−3300

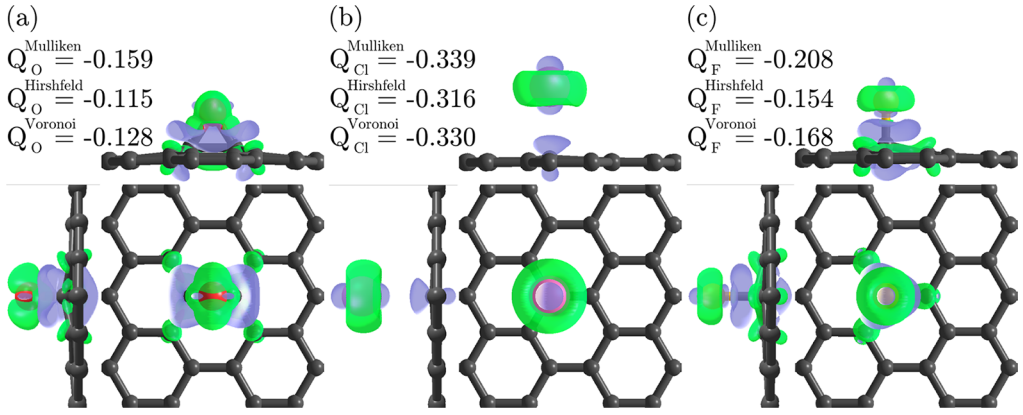


**Figure 5.** Charge transfer between graphene and (a) oxygen, (b) chlorine, and (c) fluorine adatoms evaluated through the deformation density ($\delta\rho(\mathbf{r})$). The isosurfaces are drawn for an isovalue of ±0.004 e/Å$^3$. Negative (positive) charge accumulation is displayed in green (blue). The atomic charge transfers calculated with three different methods indicate that O, Cl, and F adatoms attract electrons, which renders graphene more or less p-doped.

the deformation density, $\delta\rho(\mathbf{r})$, which is the difference between the density of the whole system ($\rho(\mathbf{r})$) and the sum of individual atomic densities ($\sum\rho_{atom}(\mathbf{r})$). The atomic charge is usually expressed as $Q_i = Z_i - \int_{at.\text{-}region}\rho(\mathbf{r})\,d\mathbf{r}$.

The application of the concept of charge transfer in the context of nanoscale carbon systems can be useful to predict, for instance, the resulting amount of doping provided by a given chemical functionalization. In Figure 5, the charge transfer between graphene and different adatoms (O, Cl, or F) is compared through the deformation density and atomic charge values. The three considered adatoms attract electrons (negative $Q_i$), meaning that graphene is p-doped. However, the efficiency of the p-doping can vary by a factor of 2 depending on the chosen functionalizing adatom. The present results confirm also that Hirshfeld and Voronoi methods give similar values and that Mulliken charges tend to be overestimated with the use of a double $\zeta$ polarized (DZP) basis set.

## 10. TUNNELING SPECTROSCOPIES AND CONDUCTANCE

Nanoscale carbon systems have been intensively investigated as potential components, either passive or active, in electronic devices. At the relevant scales of these systems, semiclassical transport models are no longer valid, and the quantum mechanical wave nature of the electrons has to be taken into consideration.

The theory of coherent quantum transport relies on Landauer's view of current as arising from the probability of electrons to go from one end of the device (e.g., the left contact) to the other (e.g., the right contact).[63−65] In this scheme, the central piece is the transmission function $T(E)$, and the current is given by

$$I = \frac{e}{h}\int_{-\infty}^{+\infty} \overbrace{T(E)}^{\text{transmission}} \underbrace{[f_L(\varepsilon - eV) - f_R(\varepsilon)]}_{\text{Fermi-Dirac distribution}} d\varepsilon \qquad (4)$$

In this formulation, the device is spatially partitioned in three regions: the source and drain leads, assumed to be periodic semi-infinite, and the central region where all scattering processes take place. The calculation of the transmission function can be equally performed using standard scattering theory or by means of Green's function techniques.[66,67]

The quantum conductance of a pristine ANR (dotted line in Figure 6a−e) exhibits plateaus associated with the quantized

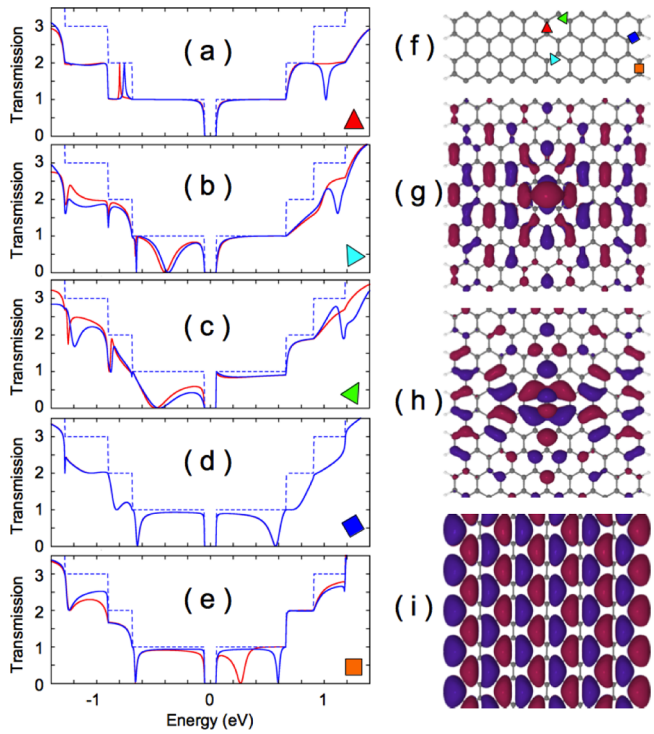


**Figure 6.** (a−e) Conductance as a function of energy for different positions of an adatom relative to the edge as depicted in panel f. Blue and red curves are associated with the two independent spin orientations. (g, h) Representation of the quasi-localized states due to the centered adatom, which are orthogonal to the low energy transmission channel depicted in panel i. Blue and red colors are associated with isosurfaces of opposite isovalues.

conductance of each ballistic conduction channel. Perturbations, such as topological defects, adatoms, or impurities, introduce quasi-localized states that may scatter the carriers incoming from the leads. Backscattering generally introduces dips in the transmission function around the eigenenergies of the quasi-localized states. The scattering profile of a given perturbation strongly depends on its structural and chemical characteristics as is illustrated in Figure 6a−f for the case of


dx.doi.org/10.1021/ar500281v | Acc. Chem. Res. 2014, 47, 3292−3300

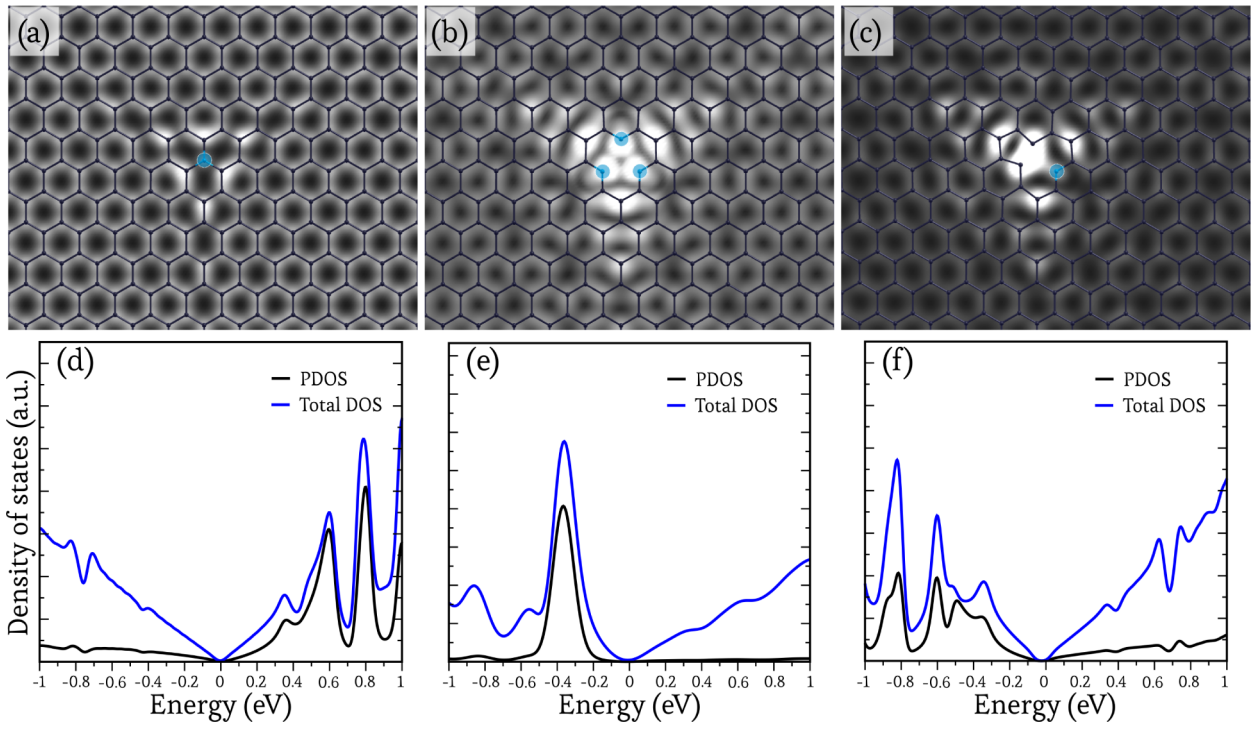


**Figure 7.** Simulated STM images of graphene doped with nitrogen in different configurations: (a) single substitution; (b) pyridinic; (c) vacancy–substitution complex. Panels d, e, and f show the total and projected density of states close to the nitrogen sites of images a, b and c, respectively. The PDOS represents the fingerprint of each defect, and can be associated with experimental STS.

carbon adatom in a nanoribbon. A special case arises when the localized state (Figure 6g,h) is orthogonal to the incoming states (see Figure 6i). In this configuration, the defect induced localized state has no cross section with the transmission eigenchannel. Hence, the carriers may still propagate ballistically. This is the case when the adatom is centered on the longitudinal axis of the ANR.[41]

The same Landauer methodology applies successfully to the simulation of tunneling microscopies. In scanning-tunneling microscopy/spectroscopy (STM/STS), a metallic tip is brought close to the sample's surface under low temperature and pressure conditions. When the tip is close enough (a few angstroms), the tunneling resistance drops and a current is measurable. If the tip scans the surface and its height is adjusted to maintain a constant current, information about the topography of the surface is obtained. If the tip is held at a constant position but the bias between the sample and the tip is varied, information about the density of electronic states is acquired. The tunneling current between a metallic tip and a surface can be computed as in eq 4. The transfer matrix would now represent the tunneling transmission from the electronic states of the surface to the those of the tip. In the Tersoff and Hamann approximation, the tip is considered as a perfect metallic tip with a spherical orbital, such that the transfer matrix and the electronic density of the tip are reduced to constants.[68] Therefore, the current is proportional to the sample's GS electronic density integrated in a region of energy that is correlated with the sample–tip bias in the experiment.

Figure 7 shows three examples of nitrogen incorporation in the graphene plane. The simulated STM images of the single substitution and the pyridinic triple substitution show the same trigonal symmetry. Thus, depending on the experimental conditions, the assignment of a particular defect can be far from trivial (e.g., compare with Figure 2A of ref 69). In contrast, the defect of Figure 7c is easier to identify with that of Figure 4c of ref 70. Therefore, it has been stressed that an unambiguous identification of defects should be carried out by comparison of both STM and STS simulation and experiment.[71]

## 11. CONCLUDING REMARKS

The catalog of physical properties accessible from DFT is abundant, and many problems of materials science can be tackled within such a framework. Beyond contributing to the understanding of $sp^2$ systems, simulations from first-principles have also provided insight into the mechanical, chemical, and electronic properties of carbon nanostructures. Hence, DFT has been very important to the advancement of carbon science. Yet, new properties of new forms of carbon continue to excite the scientist's curiosity and imagination. Therefore, the landscape of possibilities that lies in front of $sp^2$ carbon science guarantees that the field will continue to use and profit from DFT-aided experiments.

## ■ AUTHOR INFORMATION

### Corresponding Author

*E-mail: andres.botello@uclouvain.be.

### Notes

The authors declare no competing financial interest.

### Biographies

**Dr. Andrés R. Botello-Méndez** received his Ph.D. in Applied Sciences (Nanoscience and Nanotechnology) in 2009 from IPICYT (Mexico). After a postdoctoral scholarship from the Marcel de Merre prize of Louvain (Belgium), he received his current mandate as Chargé de Recherches from FNRS (Belgium). He is mainly involved in

theoretical and experimental studies of the properties of two-dimensional materials.

**Dr. Simon M.-M. Dubois** received his Ph.D. in Materials Sciences in 2010 from Université catholique de Louvain (Belgium). After a stay as Post-Doctoral Research Associate in the Cavendish laboratory, he returned in 2013 to his Alma Matter. His main research interests are in the area of quantum transport and large-scale first-principles simulations.

**Dr. Aurélien Lherbier** received his Ph.D. in Condensed Matter and Radiation Physics in 2008 from Université Joseph Fourier (France). After a first postdoctoral reasearch of two years, he is currently in the 4th year of his current mandate as Chargé de Recherches from FNRS (Belgium). His main research interest is dedicated to multiscale simulations of transport properties in nanoscale materials.

**Prof. Jean-Christophe Charlier** is Professor at the Institute of Condensed Matter and Nanosciences (University of Louvain). His main scientific interests are centered on theoretical condensed matter physics and nanosciences, first-principles computer modeling of graphene and related carbon nanostructures, and ab initio quantum transport through single molecules and other nanosystems.

## ■ ACKNOWLEDGMENTS

A.R.B.-M., A.L. and J.C.C. acknowledge the National Fund for Scientific Research [F.R.S.-FNRS] of Belgium for financial support. This research is connected to the ARC Graphene Nanoelectromechanics (No. 11/16-037) and to the ICT FET Flagship on Graphene entitled "Graphene-based revolutions in ICT and beyond". Computational resources are provided by the UCL-CISM.

## ■ REFERENCES

(1) Born, M.; Oppenheimer, R. Zur quantentheorie der molekeln. *Ann. Phys.* **1927**, *389*, 457−484.
(2) Hohenberg, P.; Kohn, W. Inhomogeneous electron gas. *Phys. Rev.* **1964**, *136*, B864−B871.
(3) Kohn, W. Nobel Lecture: Electronic structure of matterwave functions and density functionals. *Rev. Mod. Phys.* **1999**, *71*, 1253−1266.
(4) Kohn, W.; Sham, L. J. Self-Consistent Equations Including Exchange and Correlation Effects. *Phys. Rev.* **1965**, *140*, A1133−A1138.
(5) Payne, M. C.; Teter, M. P.; Allan, D. C.; Arias, T. A.; Joannopoulos, J. D. Iterative minimization techniques for ab initio total-energy calculations: molecular dynamics and conjugate gradients. *Rev. Mod. Phys.* **1992**, *64*, 1045−1097.
(6) Barth, U. v. Basic Density-Functional Theoryan Overview. *Phys. Scr.* **2004**, *2004*, No. 9.
(7) Onida, G.; Reining, L.; Rubio, A. Electronic excitations: Density-functional versus many-body Greens-function approaches. *Rev. Mod. Phys.* **2002**, *74*, 601−659.
(8) Gonze, X. First-principles responses of solids to atomic displacements and homogeneous electric fields: Implementation of a conjugate-gradient algorithm. *Phys. Rev. B* **1997**, *55* (16), 10337−10354.
(9) Baroni, S.; de Gironcoli, S.; Dal Corso, A.; Giannozzi, P. Phonons and related crystal properties from density-functional perturbation theory. *Rev. Mod. Phys.* **2001**, *73*, 515−562.
(10) Møller, C.; Plesset, M. S. Note on an approximation treatment for many-electron systems. *Phys. Rev.* **1934**, *46*, 618−622.
(11) Bloch, F. Ber die quantenmechanik der elektronen in kristallgittern. *Z. Phys.* **1929**, *52*, 555−600.
(12) Blase, X.; Rubio, A.; Louie, S. G.; Cohen, M. L. Quasiparticle band structure of bulk hexagonal boron nitride and related systems. *Phys. Rev. B* **1995**, *51*, 6868−6875.
(13) Trevisanutto, P. E.; Giorgetti, C.; Reining, L.; Ladisa, M.; Olevano, V. Ab initio GW many-body effects in graphene. *Phys. Rev. Lett.* **2008**, *101*, No. 226405.
(14) Hellmann, H. *Einfuhrung in die quantenchemie*; Franz Deuticke: Leipzig, Germany, 1937.
(15) Feynman, R. P. Forces in Molecules. *Phys. Rev.* **1939**, *56*, 340−343.
(16) Haas, P.; Tran, F.; Blaha, P. Calculation of the lattice constant of solids with semilocal functionals. *Phys. Rev. B* **2009**, *79*, No. 085104.
(17) Ceperley, D. M.; Alder, B. J. Ground state of the electron gas by a stochastic method. *Phys. Rev. Lett.* **1980**, *45*, 566−569.
(18) Perdew, J. P.; Burke, K.; Ernzerhof, M. Generalized gradient approximation made simple. *Phys. Rev. Lett.* **1996**, *77*, 3865−3868.
(19) Perdew, J. P.; Ruzsinszky, A.; Csonka, G. I.; Vydrov, O. A.; Scuseria, G. E.; Constantin, L. A.; Zhou, X.; Burke, K. Restoring the density-gradient expansion for exchange in solids and surfaces. *Phys. Rev. Lett.* **2008**, *100*, No. 136406.
(20) Dion, M.; Rydberg, H.; Schröder, E.; Langreth, D. C.; Lundqvist, B. I. Van der Waals density functional for general geometries. *Phys. Rev. Lett.* **2004**, *92*, No. 246401.
(21) Klimes, J.; Bowler, D. R.; Michaelides, A. Chemical accuracy for the van der Waals density functional. *J. Phys.: Condens. Matter* **2010**, *22*, No. 022201.
(22) Lee, K.; Murray, D.; Kong, L.; Lundqvist, B. I.; Langreth, D. C. Higher-accuracy van der Waals density functional. *Phys. Rev. B* **2010**, *82*, No. 081101.
(23) Hull, A. W. A new method of X-ray crystal analysis. *Phys. Rev.* **1917**, *10*, 661−696.
(24) Zacharia, R.; Ulbricht, H.; Hertel, T. Interlayer cohesive energy of graphite from thermal desorption of polyaromatic hydrocarbons. *Phys. Rev. B* **2004**, *69*, No. 155406.
(25) Vanin, M.; Mortensen, J. J.; Kelkkanen, A. K.; Garcia-Lastra, J. M.; Thygesen, K. S.; Jacobsen, K. W. Graphene on metals: A van der Waals density functional study. *Phys. Rev. B* **2010**, *81*, No. 081408.
(26) Hamada, I.; Otani, M. Comparative van der Waals density-functional study of graphene on metal surfaces. *Phys. Rev. B* **2010**, *82*, No. 153412.
(27) von Barth, U.; Hedin, L. A local exchange-correlation potential for the spin polarized case. i. *J. Phys. C: Solid State Phys.* **1972**, *5*, 1629−1642.
(28) Rajagopal, A. K.; Callaway, J. Inhomogeneous electron gas. *Phys. Rev. B* **1973**, *7*, 1912−1919.
(29) Yazyev, O. V. Emergence of magnetism in graphene materials and nanostructures. *Rep. Prog. Phys.* **2010**, *73*, No. 056501.
(30) Wehling, T. O.; Lichtenstein, A. I.; Katsnelson, M. I. Transition-metal adatoms on graphene: Influence of local Coulomb interactions on chemical bonding and magnetic moments. *Phys. Rev. B* **2011**, *84*, No. 235110.
(31) Yazyev, O. V.; Helm, L. Defect-induced magnetism in graphene. *Phys. Rev. B* **2007**, *75*, No. 125408.
(32) Son, Y.-W.; Cohen, M. L.; Louie, S. G. Energy gaps in graphene nanoribbons. *Phys. Rev. Lett.* **2006**, *97*, No. 216803.
(33) Botello-Méndez, A. R.; Declerck, X.; Terrones, M.; Terrones, H.; Charlier, J.-C. One-dimensional extended lines of divacancy defects in graphene. *Nanoscale* **2011**, *3*, 2868−2872.
(34) Alexandre, S. S.; Lcio, A. D.; Neto, A. H. C.; Nunes, R. W. Correlated Magnetic States in Extended One-Dimensional Defects in Graphene. *Nano Lett.* **2012**, *12*, 5097−5102.
(35) Konschuh, S.; Gmitra, M.; Fabian, J. Tight-binding theory of the spin-orbit coupling in graphene. *Phys. Rev. B* **2010**, *82*, No. 245412.
(36) Pesin, D.; MacDonald, A. H. Spintronics and pseudospintronics in graphene and topological insulators. *Nat. Mater.* **2012**, *11*, 409−416.
(37) Roche, S.; Valenzuela, S. O. Graphene spintronics: Puzzling controversies and challenges for spin manipulation. *J. Phys. D: Appl. Phys.* **2014**, *47*, No. 094011.
(38) Dresselhaus, G.; Dresselhaus, M. S. Spin-orbit interaction in graphite. *Phys. Rev.* **1965**, *140*, A401−A412.

(39) Huertas-Hernando, D.; Guinea, F.; Brataas, A. Spin-orbit coupling in curved graphene, fullerenes, nanotubes, and nanotube caps. *Phys. Rev. B* **2006**, *74*, No. 155426.
(40) Gmitra, M.; Kochan, D.; Fabian, J. Spin-orbit coupling in hydrogenated graphene. *Phys. Rev. Lett.* **2013**, *110*, No. 246602.
(41) Dubois, S. Quantum Transport in Molecular Junctions and Graphene Based Nanostructures, Ph.D. Thesis, UCL, Louvain-la-Neuve, 2010.
(42) Bailey, C. L.; Wander, A.; Mukhopadhyay, S.; Searle, B. G.; Harrison, N. M. *Ab Initio Surface Thermodynamics in Multi Component Environments*; Science and Technology Facilities Council: Warrington, U.K., 2007.
(43) Şahin, H.; Ciraci, S. Chlorine adsorption on graphene: Chlorographene. *J. Phys. Chem. C* **2012**, *116*, 24075−24083.
(44) Mills, G.; Jónsson, H. Quantum and thermal effects in $H_2$ dissociative adsorption: Evaluation of free energy barriers in multidimensional quantum systems. *Phys. Rev. Lett.* **1994**, *72*, 1124−1127.
(45) Henkelman, G.; Uberuaga, B. P.; Jnsson, H. A climbing image nudged elastic band method for finding saddle points and minimum energy paths. *J. Chem. Phys.* **2000**, *113*, 9901−9904.
(46) Özçelik, V. O.; Cahangirov, S.; Ciraci, S. Epitaxial growth mechanisms of graphene and effects of substrates. *Phys. Rev. B* **2012**, *85*, No. 235456.
(47) Sheppard, D.; Terrell, R.; Henkelman, G. Optimization methods for finding minimum energy paths. *J. Chem. Phys.* **2008**, *128*, No. 134106.
(48) Dresselhaus, M.; Dresselhaus, G.; Saito, R.; Jorio, A. Raman spectroscopy of carbon nanotubes. *Phys. Rep.* **2005**, *409*, 47−99.
(49) Dresselhaus, M. S.; Jorio, A.; Hofmann, M.; Dresselhaus, G.; Saito, R. Perspectives on carbon nanotubes and graphene Raman spectroscopy. *Nano Lett.* **2010**, *10*, 751−758.
(50) Popov, V. N.; Van Doren, V. E.; Balkanski, M. Elastic properties of single-walled carbon nanotubes. *Phys. Rev. B* **2000**, *61*, 3078−3084.
(51) Salvetat-Delmotte, J.-P.; Rubio, A. Mechanical properties of carbon nanotubes: A fiber digest for beginners. *Carbon* **2002**, *40*, 1729−1734.
(52) Wagner, P.; Ivanovskaya, V. V.; Rayson, M. J.; Briddon, P. R.; Ewels, C. P. Mechanical properties of nanosheets and nanotubes investigated using a new geometry independent volume definition. *J. Phys.: Condens. Matter* **2013**, *25*, No. 155302.
(53) Savini, G.; Dappe, Y. J.; Öberg, S.; Charlier, J. C.; Katsnelson, M. I.; Fasolino, A. Bending modes, elastic constants and mechanical stability of graphitic systems. *Carbon* **2011**, *49*, 62−69.
(54) de Andres, P. L.; Guinea, F.; Katsnelson, M. I. Density functional theory analysis of flexural modes, elastic constants, and corrugations in strained graphene. *Phys. Rev. B* **2012**, *86*, No. 245409.
(55) Tan, P. H.; Han, W. P.; Zhao, W. J.; Wu, Z. H.; Chang, K.; Wang, H.; Wang, Y. F.; Bonini, N.; Marzari, N.; Pugno, N.; Savini, G.; Lombardo, A.; Ferrari, A. C. The shear mode of multilayer graphene. *Nat. Mater.* **2014**, *4*, 294−300.
(56) Mulliken, R. S. Electronic population analysis on LCAOMO molecular wave Functions. I. *J. Chem. Phys.* **1955**, *23*, 1833−1840.
(57) Mulliken, R. S. Spectroscopy, molecular orbitals, and chemical bonding. *Nobel Lectures, Chemistry 1963−1970*; World Scientific: Singapore, 1966; p 131.
(58) Fonseca Guerra, C.; Handgraaf, J.-W.; Baerends, E. J.; Bickelhaupt, F. M. Voronoi deformation density (VDD) charges: Assessment of the Mulliken, Bader, Hirshfeld, Weinhold, and VDD methods for charge analysis. *J. Comput. Chem.* **2004**, *25*, 189−210.
(59) Hirshfeld, F. Bonded-atom fragments for describing molecular charge densities. *Theor. Chim. Acta* **1977**, *44*, 129−138.
(60) Bader, R. F. W. *Atoms in Molecules: A Quantum Theory*; Oxford University Press: Oxford, 1994.
(61) Henkelman, G.; Arnaldsson, A.; Jnsson, H. A fast and robust algorithm for Bader decomposition of charge density. *Comput. Mater. Sci.* **2006**, *36*, 354−360.
(62) Bickelhaupt, F. M.; van Eikema Hommes, N. J. R.; Fonseca Guerra, C.; Baerends, E. J. The carbon−lithium electron pair bond in $(CH_3Li)_n$ ($n$ = 1, 2, 4). *Organometallics* **1996**, *15*, 2923−2931.
(63) Landauer, R. Spatial variation of currents and fields due to localized scatterers in metallic conduction. *IBM J. Res. Dev.* **1957**, *1*, 223−231.
(64) Landauer, R. Electrical resistance of disordered one-dimensional lattices. *Philos. Mag.* **1970**, *21*, 863−867.
(65) Landauer, R. Electrical transport in open and closed systems. *Z. Phys. B: Condens. Matter* **1987**, *68*, 217−228.
(66) Datta, S. *Quantum Transport: Atom to Transistor*; Cambridge University Press: Cambridge, 2005.
(67) Sancho, M. P. L.; Sancho, J. M. L.; Sancho, J. M. L.; Rubio, J. Highly convergent schemes for the calculation of bulk and surface Green functions. *J. Phys. F: Met. Phys.* **1985**, *15*, 851−858.
(68) Tersoff, J.; Hamann, D. R. Theory and application for the scanning tunneling microscope. *Phys. Rev. Lett.* **1983**, *50*, 1998−2001.
(69) Zhao, L.; He, R.; Rim, K.-T.; Schiros, T.; Kim, K.-S.; Zhou, H.; Gutiérrez, C.; Chockalingam, S. P.; Arguello, C. J.; Pálová, L.; Nordlund, D.; Hybertsen, M.; Reichman, D. R.; Heinz, T. F.; Kim, P.; Pinczuk, A.; Flynn, G. W.; Pasupathy, A. N. Visualizing individual nitrogen dopants in monolayer graphene. *Science* **2011**, *333*, 999−1003.
(70) Deng, D.; Pan, X.; Yu, L.; Cui, Y.; Jiang, Y.; Qi, J.; Li, W.-X.; Fu, Q.; Ma, X.; Xue, Q.; Sun, G.; Bao, X. Toward n-doped graphene via solvothermal synthesis. *Chem. Mater.* **2011**, *23*, 1188−1193.
(71) Lv, R.; Li, Q.; Botello-Méndez, A. R.; Hayashi, T.; Wang, B.; Berkdemir, A.; Hao, Q.; Elías, A. L.; Cruz-Silva, E.; Gutiérrez, H. R.; Kim, Y.-A.; Muramatsu, H.; Zhu, J.; Endo, M.; Terrones, H.; Charlier, J.-C.; Pan, M.; Terrones, M. Nitrogen-doped graphene: Beyond single substitution and enhanced molecular sensing. *Sci. Rep.* **2012**, *2*, No. 586.